9

Three-Dimensional Numerical Analyses on Liquid-Metal Magnetohydrodynamic Flow Through Circular Pipe in Magnetic-Field Outlet-Region

Hiroshige Kumamaru, Kazuhiro Itoh and Yuji Shimogonya
University of Hyogo
Japan

1. Introduction

In conceptual design examples of a fusion reactor power plant, a lithium-bearing blanket in which a great amount of heat is produced is cooled mainly by helium gas, water or liquid-metal lithium (Asada et al. Ed., 2007). The liquid-metal lithium is an excellent coolant having high heat capacity and thermal conductivity and also can breed tritium that is used as fuel of a deuterium-tritium (D-T) fusion reactor. In cooling the blanket, however, the liquid-metal lithium needs to pass through a strong magnetic field that is used to magnetically confine high-temperature reacting plasma in a fusion reactor core. There exists a large magnetohydrodynamic (MHD) pressure drop arising from the interaction between the liquid-metal flow and the magnetic field. In particular, the MHD pressure drop becomes considerably larger in the inlet region or outlet region of the magnetic field than in the fully-developed region inside the magnetic field for the reason mentioned later in this chapter.

A three-dimensional calculation is indispensable for the exact calculation of MHD channel flow in the inlet region or outlet region of magnetic field, also as described later in this chapter. There exist a few three-dimensional numerical calculations on the MHD flows in rectangular channels with a rectangular obstacle (Kalis and Tsinober, 1973), with abrupt widening (Itov et al., 1983), or with turbulence promoter such as conducting strips (Leboucher, 1999). All these calculations, however, were carried out for low Hartmann numbers (corresponding to low strength of the applied magnetic field) and low Reynolds number, because of instability problems in numerical calculations.

As to the MHD channel flow in the magnetic-field inlet-region, three-dimensional numerical calculations were conducted for the cases of Hartmann number of ~10 and Reynolds number of ~100 (Khan and Davidson, 1979). The calculations were based on what is called the parabolic approximation, in which the flow and magnetic field effects are assumed to transfer only in the main flow direction. However, the calculations based on parabolic approximation cannot predict exactly the MHD flow in the magnetic-field inlet-region. Were performed full three-dimensional calculations (without any assumptions) on the MHD rectangular-channel flow in the magnetic-field inlet-region (Sterl, 1990). The calculations

were conducted mainly for the ranges of Hartmann numbers from 50 to 70 and Reynolds numbers from 2.5 to 5, and for a smoothly-increasing applied magnetic field. However, these ranges of Reynolds numbers and Hartmann numbers are unrealistic as conditions that appear even in laboratory conditions. The laboratory conditions reach Reynolds numbers up to ~1000 and Hartmann numbers up to ~100 simultaneously.

In fusion reactor conditions, the Reynolds number and the Hartmann number reach ~10^4 and ~10^4, respectively, the channel walls are electrically-conducting, the magnetic field changes in steps at the inlet or the outlet, and the flow changes from non-MHD turbulent flow to MHD laminar flow. However, because of instability problems in numerical calculations, it is quite difficult to obtain three-dimensional numerical solutions on MHD flows in the magnetic-field inlet-region or outlet-region even in the laboratory conditions that reach Reynolds numbers up to ~1000 and Hartmann numbers up to ~100 simultaneously.

Within the present limit of computer performance, the authors have already performed full three-dimensional calculations on the MHD flow through a circular pipe in the magnetic-field inlet-region, in simulating typical laboratory conditions (Kumamaru et al., 2007). In the calculations, the Hartmann number and the Reynolds number are ~100 and ~1000, respectively, the channel walls are electrically-insulating, the applied magnetic field changes in steps, and a laminar non-MHD flow enters the calculation domain. In this study, full three-dimensional calculations are performed on the MHD flow through a circular pipe in the magnetic-field outlet-region for the same conditions as for the magnetic-field inlet-region.

Figure 1 shows schematically the coordinate system, the applied magnetic field and the induced electric currents, together with the directions of Lorentz force, in the outlet region of the magnetic field. The applied magnetic field is imposed in the y direction, having a constant value for z=0~$z1$, a linear decrease from z=$z1$~$z2$, and a value of zero for z=$z2$~$z0$, as shown in Fig. 1(a).

In the region of fully-developed MHD flow near z=0, the induced electric current which is produced by the vector product of flow velocity and applied magnetic field flows in the negative x direction as shown in Figs. 1(b) and 1(c1). The induced current returns by passing through regions very near the walls (in an x-y plane at the same z) where the flow velocity is nearly zero, in the case of insulating walls. (The induced current can also pass through the walls in the case of conducting walls.) The induced current loop has a relatively large electrical resistance, since the current needs to flow in the thin regions near the walls. The Lorentz force which is caused by the vector product of induced current and applied magnetic field acts in the negative z direction and produces a large pressure drop.

In the outlet region of magnetic field from $z \approx z1$ to $z \approx z2$, the induced electric current flows in the negative x direction, as was the case of fully-developed region, as shown in Fig. 1(b).

However, the induced current can pass through the large region downstream the magnetic field section (in an x-z plane with the same y) where no magnetic field or small magnetic field is applied. The electric resistance in this region is much smaller than the resistance in the thin region near the walls mentioned above. Hence, the induced current becomes larger in the outlet region than in the fully-developed region. The Lorentz force and thus the

pressure drop also may become considerably larger in the outlet region than in the fully-developed region (Moreau, 1990).

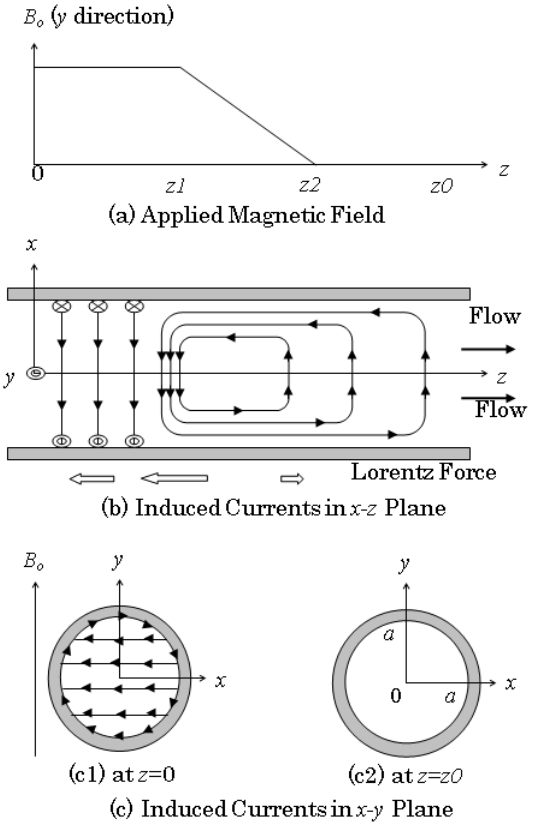

Fig. 1. Coordinate system for magnetic-field outlet-region.

On the other hand, the induced current in the last section of the outlet region near z=$z2$ can flow in the positive x direction as shown in Fig. 1(b). Thus, a smaller Lorentz force may act in the flow direction and thus a small pressure recovery may occur in this section of the outlet region (Moreau, 1990).

The induced electric currents in the outlet region, flowing in both x- and z-directions and in y-direction, cannot be calculated by a two-dimensional model. It is also important that a sufficiently large fluid region downstream the magnetic field section is included in a calculation domain. For these reasons, in this study, in order to obtaine mainly the pressure drop quantitatively, the authors have performed three-dimensional numerical calculations on the MHD flow through a circular pipe in the outlet region of the magnetic field, including the region of no magnetic field downstream the magnetic field region. To the authors' knowledge, there have been no numerical calculations or experimental studies on

the MHD flow through a circular pipe in the magnetic-field outlet-region. In this study, calculation results on the magnetic-field outlet-region have also been compared with authors' calculation results on the magnetic-field inlet-region.

2. Numerical analyses

Numerical calculations are performed for an MHD flow in a circular pipe with an inner radius of *a*, shown in Fig. 1. A fully-developed MHD laminar flow enters the calculation domain at *z*=0, and a fully-developed non-MHD flow leaves the domain at *z*=*z0*. The applied magnetic field is imposed in the *y* direction as shown in Fig. 1(a), as was stated previously.

The basic equations which describe a liquid-metal MHD flow are the continuity equation, the momentum equation and the induction equation. The equations are expressed respectively by:

$$\nabla \cdot \boldsymbol{v} = 0\,, \tag{1}$$

$$\rho\left[\frac{\partial \boldsymbol{v}}{\partial t} + (\boldsymbol{v}\cdot\nabla)\boldsymbol{v}\right] = -\nabla p + \eta\nabla^2\boldsymbol{v} + \frac{1}{\mu}(\nabla\times\boldsymbol{B})\times\boldsymbol{B_0}\,, \tag{2}$$

$$\frac{\partial \boldsymbol{B}}{\partial t} = \nabla\times\left(\boldsymbol{v}\times\boldsymbol{B_0}\right) + \frac{1}{\sigma\mu}\nabla^2\boldsymbol{B}\,. \tag{3}$$

Here, $\boldsymbol{v}$ is velocity vector, p pressure, $\boldsymbol{B}$ induced magnetic field vector and t time; $\boldsymbol{B_0}$ is applied magnetic field vector, and ρ is density, η viscosity, μ magnetic permeability and σ electric conductivity. The vector $\boldsymbol{B}$ is an induced magnetic field produced by the induced electric current, and is treated as an unknown variable together with the velocity $\boldsymbol{v}$ and the pressure p. The induced electric current $\boldsymbol{j}$ can be calculated by the Ampere equation $\boldsymbol{j} = (1/\mu)(\nabla\times\boldsymbol{B})$ from $\boldsymbol{B}$. The third term in the right-hand side of Eq. (2) represents the Lorentz force. The induction equation, i.e. Eq. (3), is derived from Maxwell's equations and Ohm's law in electromagnetism.

The basic equations are expressed in nondimensional forms by introducing the following nondimensional variables (indicated by superscript *) and nondimentional numbers:

$$t^* = \frac{t}{a/\bar{v}_z},\quad r^* = \frac{r}{a},\quad z^* = \frac{z}{a},$$

$$v_r^* = \frac{v_r}{\bar{v}_z},\quad v_\theta^* = \frac{v_\theta}{\bar{v}_z},\quad v_z^* = \frac{v_z}{\bar{v}_z},\quad p^* = \frac{p}{\rho\bar{v}_z^2},$$

$$B_r^* = \frac{B_r}{\bar{v}_z\mu\sqrt{\sigma\eta}},\quad B_\theta^* = \frac{B_\theta}{\bar{v}_z\mu\sqrt{\sigma\eta}},\quad B_z^* = \frac{B_z}{\bar{v}_z\mu\sqrt{\sigma\eta}}, \tag{4}$$

$$Re = \frac{\overline{v}_z a}{\nu}, \quad Ha = B_0 a\sqrt{\frac{\sigma}{\eta}}, \quad Rm = \frac{\overline{v}_z a}{\nu_m}. \tag{5}$$

Here, r, θ, z are coordinates in the cylindrical coordinate systen; $\overline{v}_z$ mean velocity in z-direction, ν kinematic viscosity and ν_m ($=1/\sigma\mu$) magnetic kinematic viscosity. Nondimensional numbers Re, Ha and Rm are Reynolds number, Hartmann number and magnetic Reynolds number, respectively. The final nondimensional basic equations become respectively:

$$\nabla \cdot \boldsymbol{v} = 0, \tag{6}$$

$$\frac{\partial \boldsymbol{v}}{\partial t} + (\boldsymbol{v}\cdot\nabla)\boldsymbol{v} = -\nabla p + \frac{1}{Re}\nabla^2 \boldsymbol{v} + \frac{1}{Re}(\nabla \times \boldsymbol{B}) \times \boldsymbol{Ha}, \tag{7}$$

$$\frac{\partial \boldsymbol{B}}{\partial t} = \frac{1}{Rm}\nabla \times (\boldsymbol{v} \times \boldsymbol{Ha}) + \frac{1}{Rm}\nabla^2 \boldsymbol{B}. \tag{8}$$

Superscript * is omitted to simplify the description in Eqs. (6) through (8) and in the following description. Note that the Hartmann number $\boldsymbol{Ha}$ is a given (known) vector having only y-component as a given function of z, i.e. $Ha(z)$.

The coordinate system is transformed from the Cartesian coordinate system (x, y, z) to the curvilinear coordinate system (ξ, η, ζ) in order to deal with a channel with an arbitrary flow cross-section in the future, and is thereafter transformed into the cylindrical coordinate system (r, θ, z) as a special case of the curvilinear coordinate system. Considering the symmetry, the numerical calculations are carried out for the region of $0<r<1$ and $0<\theta<\pi/2$. (Note that the inner surface of the wall corresponds to $r=1$ ($x=1$ or $y=1$) in the nondimensional coordinates.)

As the boundary condition on the flow velocities, the inflow boundary condition is adopted at the flow inlet, i.e. at $z=0$, by fixing a fully-developed MHD flow velocity (Kumamaru & Fujiwara, 1999). The outflow boundary condition is given at the flow outlet, i.e. at $z=z0$, by fixing the reference pressure. No-slip condition is given at the wall and the symmetry condition is adopted at $\theta=0$ and $\theta=\pi/2$. As the boundary condition on the induced magnetic fields, $\partial B/\partial z = 0$ and $\boldsymbol{B}=0$ are specified at the flow inlet and the flow outlet, respectively. The former reflects the situation that the induced current does not change in the z-direction at the flow inlet in a fully-developed MHD flow region, and the latter represents that no induced current exists at the flow outlet in a fully-developed non-MHD flow region. At the wall, $\boldsymbol{B}=0$ is specified assuming that the walls are electrically insulating (nonconducting). The boundary conditions on the induced magnetic fields at the symmetry plane of $\theta=0$ and $\theta=\pi/2$ are not intuitively clear. Hence, by performing a calculation for the whole cross section in the case of small Hartmann numbers, it has been confirmed that the conditions are given by:

$$\theta = 0: \; A(-\theta) = -A(\theta), B(-\theta) = B(\theta), C(-\theta) = -C(\theta), \tag{9a}$$

$$\theta = \pi/2: \quad A(\pi/2-\theta) = -A(\pi/2+\theta), B(\pi/2-\theta) = B(\pi/2+\theta), C(\pi/2-\theta) = C(\pi/2+\theta), \tag{9b}$$

where A, B and C are the x, y and z components of $\boldsymbol{B}$, respectively.

The discretization of the equations is carried out by the finite difference method. The calculations are performed using a non-uniform expanding 15 x 15 x 30 grid with grid elements closely spaced near the channel wall of r=1 and the region between or around z=$z1$ and z=$z2$. The first-order accurate upwind differencing is adopted for the fluid convection terms in Eq. (7). The solution procedure follows the MAC method that is widely used in numerical calculations.

Even for the fully-developed region, it is difficult to obtain a stable numerical solution for large Hartmann numbers (Kumamaru & Fujiwara, 1999). In the present three-dimensional calculations, stable numerical solutions have been obtained for Hartmann numbers up to 100 and Reynolds numbers up to 1000 by applying the following means or procedures. (1) The grids are arranged closely near the wall of r=1, i.e. at r=0.0, … , 0.95, 0.97, 0.99, 0.995, 1.0, on referring to a velocity profile of the classical Hartmann flow, i.e. fully-developed MHD flow in infinite parallel plates (Kumamaru and Fujiwara, 1999). (2) Simultaneous linear equations on the pressure, i.e. Poisson equation, are solved not by the iterative method but by the elimination method. (3) First, a solution is obtained for Re (Reynolds number) of 0.01, and thereafter Re is increased gradually to a final value, i.e. 1000.

3. Analysis results

3.1 Pressure along flow axis

Numerical calculations have been performed for a circular pipe with insulating wall under the conditions of a Reynolds number (Re) of 1000, a Hartmann number (Ha) of 100 (for the fully-developed MHD region) and a magnetic Reynolds number (Rm) of 0.001. The Hartmann number (relating to the applied magnetic field) is 100 from z=0 to $z1$, decreases linearly from z=$z1$ to $z2$, and is zero from z=$z2$ to $z0$ (See Fig. 1(a)). The values of $z1/z2$ are changed from 10/20 to 10/10.05. (Note that both $z1$ and $z0$-$z2$ are fixed to 10 in all the cases.) These values for the nondimensional numbers and parameters are selected in order to simulate those typical to laboratory scales and conditions.

Figure 2 shows calculated pressures along the flow axis, i.e. the z-axis, for the cases of $z1/z2$ from 10/20 to 10/10.05. Figure 3 presents a calculated result only for the case of $z1/z2$=10/12 as a standard case, indicated by a solid line, together with a corresponding result for the magnetic-field inlet-region, indicated by a dotted line, which will be explained in Sec. 3.4. From z=0 to $z \approx z1$, the pressure decreases steeply following the pressure drop of a fully-developed MHD flow. From $z \approx z1$ to $z \approx z2$, the pressure decreases more sharply than in the region of z<$z1$, since a large Lorentz force is produced in the negative z direction as was mentioned in Chap. 1 and again will be explained in Sec. 3.2. In z>$z2$, the pressure decreases slowly, representing the frictional pressure drop as a non-MHD laminar flow.

The steeper the gradient of the applied magnetic field becomes, the more sharply the pressure decreases from $z \approx z1$ to $z \approx z2$. However, the pressure drop through the magnetic-field outlet-region becomes saturated for the steeper gradient of the magnetic field (See the cases of $z1/z2$=10/10.1 and 10/10.05). For the slower gradient of the magnetic field, the effect of the length along the flow axis (i.e. z-axis) contributes more to the pressure drop through the outlet region than the effect of the outlet region (Compare the cases of $z1/z2$=10/20 and 10/15).

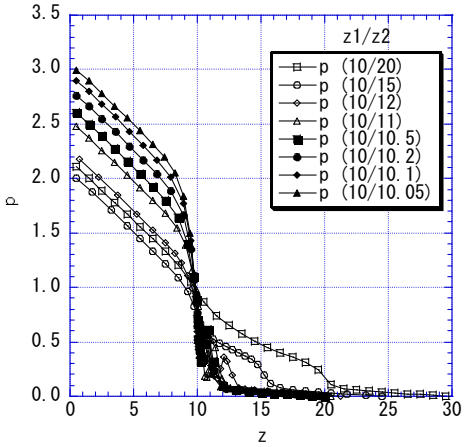

Fig. 2. Pressures along z-axis for $z1/z2$=10/20 to 10/10.05.

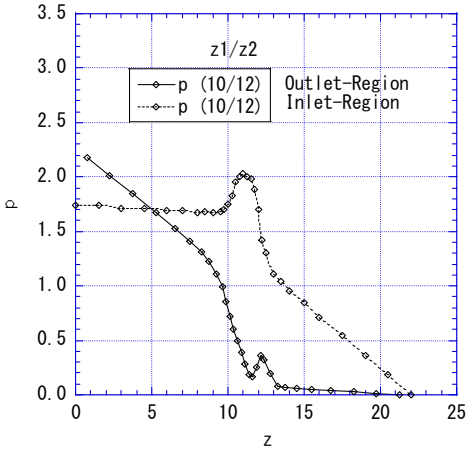

Fig. 3. Pressures along z-axis for $z1/z2$=10/12.

The small pressure recovery, which was also pointed out in Chap. 1 and again will be expained in Sec. 3.2, is observed in the region near $z \approx z2$ for the cases of $z1/z2$=10/12~10/10.05. The pressure drop appears again outside the magnetic-field region. This may be due to rapid change in velocity distibution in this region, which will be explained in Sec. 3.4.

The pressure drops in the fully-developed region of $z<z1$, $-\Delta p/\Delta z$, are almost the same for all the cases. The pressure drops agree with a value calculated numerically by the authors for the fully-developed MHD flow, $-\Delta p/\Delta z \approx 0.123$ (Kumamaru and Fujiwara, 1999), and also agree nearly with a value predicted by Schercliff's theoretical approximate equation, $-\Delta p/\Delta z \approx 0.118$ (Schercliff, 1956; Lielausis, 1975), for the case of Ha=100 and Re=1000. As

mentioned in Chap. 1, no experimental data on the pressure drop through the magnetic-field outlet-region have been reported. However, pressure drops through the magnetic-field inlet-region calculated numerically by the authers agreed nearly with those estimated by an existing equation based on experimental data (Kumamaru 2007; Lielausis, 1975).

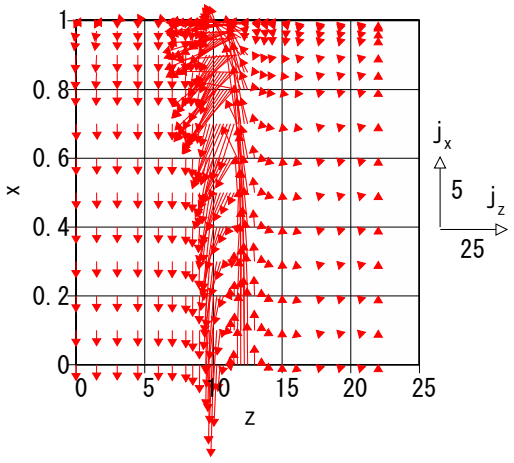

Fig. 4. Induced currents in x-z plane at y=0 for $z1/z2$=10/12.

3.2 Induced current distribution

Figure 4 illustrates induced electric current distribution in the x-z plane at y=0 for the case of $z1/z2$=10/12, i.e. the standard case. Figures 5(a), (b) and (c) give induced current distributions in the x-y planes at z=4.5, 10 and 12, respectively, for the same case. On the right side of each figure, is shown the magnitude of the (nondimensional) induced current vector in the each coordinate direction. In Figs. 5(a) through (c), the induced current vector is reduced by a factor of 4 for two vectors from the wall at each circumferential angle, in order to make the figures compact.

In the fully-developed region from z=0 to $z \approx 8$, the induced current, flowing mainly in the negative x-direction, does not change in the z-direction, as shown in Fig. 4. This constant induced current produces constant Lorentz force (acting in the negative z direction) and results in constant pressure drop along the z-axis as shown in Fig. 3. The induced current returns by passing in an extremely thin region very near the wall, as shown in Fig. 5(a). Almost no induced current (less than 10^{-2}) flows in the region from $z \approx 14$ to z=22, as shown in Fig. 4, since no magnetic field is applied.

In the magnetic-field outlet-region from $z \approx 8$ to $z \approx 14$, the induced current forms a loop mainly in the x-z plane, as shown in Fig. 4. The induced current is larger in the outlet region than in the fully-developed region. This is because the electric resistance of the induced current loop in the outlet region is much smaller than the resistance of the loop in the fully-developed region. The induced current can return in the large downstream region in the outlet region, although the current needs to return only in the extremely thin region near the wall in the fully-developed region.

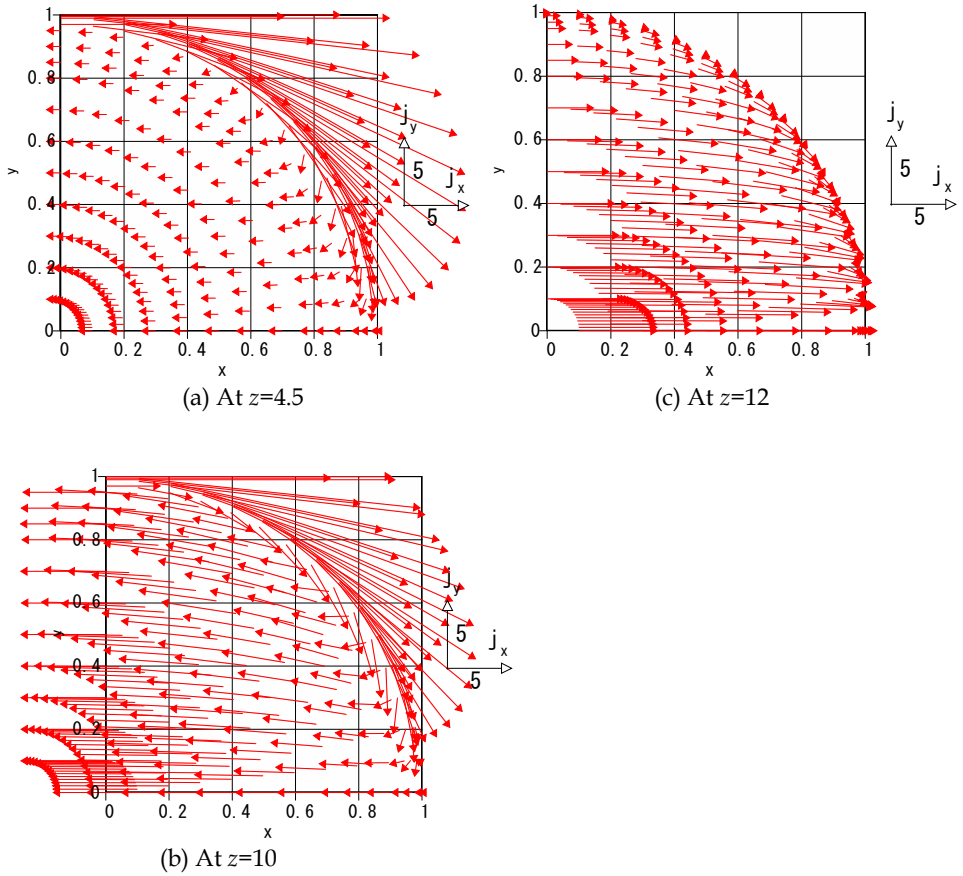

(a) At z=4.5

(c) At z=12

(b) At z=10

Fig. 5. Induced currents in x-y plane for $z1/z2$=10/12.

The induced current flows mainly in the negative x-direction from $z \approx 8$ to $z \approx 11$. Hence, in this region, a larger Lorentz force than in the fully-developed region acts in the negative z-direction, and a larger pressure drop is produced along the z-axis as shown in Fig. 3. On the other hand, the induced current flows mainly in the positive x-direction from $z \approx 11.5$ to $z \approx 13$. Thus, the Lorentz force is exerted in the positive z-direction, and a small pressure recovery along the z-axis happens from $z \approx 11.5$ to $z \approx 12$ as shown in Fig. 3. (No external magnetic field is applied from $z \approx 12$ to $z \approx 13$.) Also in the outlet region, there exists an induced current loop which returns in an extremely thin region near the wall, as shown in Fig. 5(b).

3.3 Velocity distribution

Figures 6(a), (b), (c), (d) and (e) show calculated velocity v_z distributions at z=4.5, 10, 11, 12 and 17.5, respectively, for the case of $z1/z2$=10/12, i.e. the standard case. There is no significant difference among velocity distributions from z=0 to z=8. The velocity profile is a

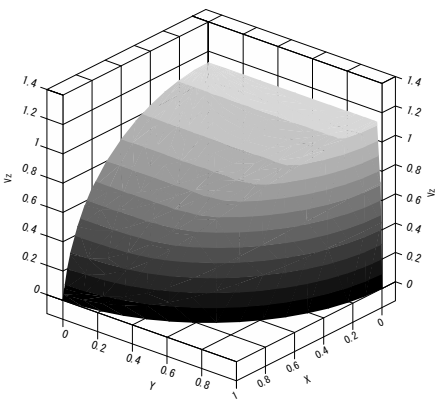

(a) At z=4.5

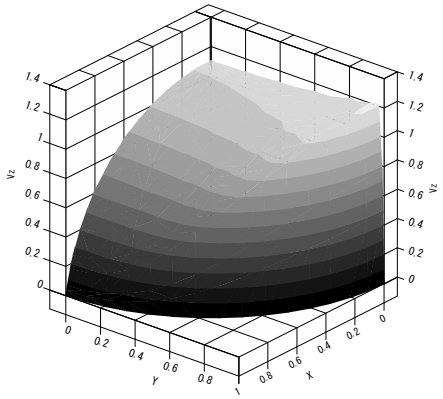

(b) At z=10

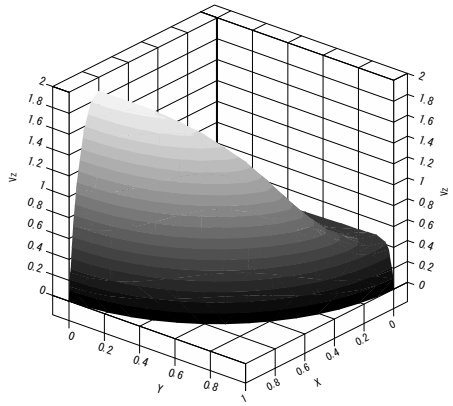

(c) At z=11

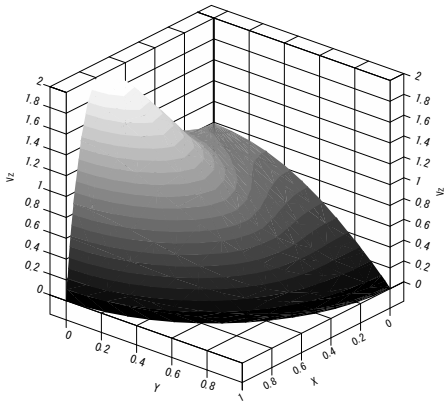

(d) At z=12

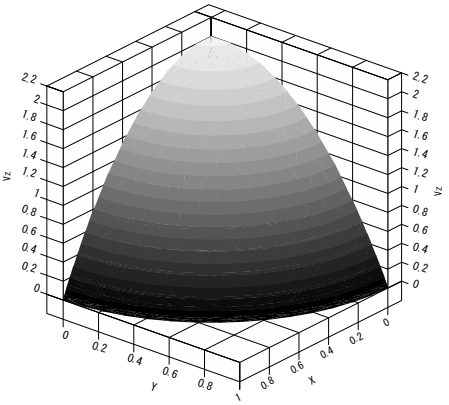

(e) At z=17.5

Fig. 6. Velocity distribution for $z1/z2$=10/12.

flat one, particularly in the direction of applied magnetic field, having a peak value of ~1.1, as shown in Fig. 6(a). The velocity distribution in this region agrees nearly with a profile calculated by the authors for the fully-developed MHD flow (Kumamaru, 1999).

The velocity distribution at z=10, shown in Fig. 6(b), is still nearly flat. The velocity profile changes sharply at $z \approx 11$ and shows what is called an M-shape distribution having a peak near the wall, as shown in Fig. 6(c). This is because the Lorentz force acting in the negative z-direction suppresses the flow in the z-direction in the fluid bulk region, though small Lorentz force acts in the negative z-direction in the region near the wall of x=1. The velocity distribution at z=12, at the outlet of applied magnetic field, shown in Fig. 6(d), is still nearly the same as that at z=11, shown in Fig. 6(c).

The velocity profile changes sharply, from z=12 to $z \approx 13$, from the M-shape distribution, shown in Fig. 6(d), to a parabolic distribution typical to a non-MHD flow, shown in Fig. 6(e). The pressure decrease from z=12 to $z \approx 13$, shown in Fig. 3, is attributable to this sharp change in velosity distribution. It is considered that the pressure decreases largely since the velocity increases quickly in the fluid bulk region. No significant difference exists among velocity profiles from $z \approx 13$ to z=22. The velocity profile is a parabolic one of a non-MHD laminar flow with a peak value of ~2.

3.4 Comparison with magnetic-field inlet-region

Figure 7 shows schematically the applied magnetic field in the y-direction, the induced currents in the x-z plane including the directions of Lorentz force and the pressure along the z-axis, in the inlet region and the outlet region of the magnetic field. The larger Lorentz force acts and thus the larger pressure drop occurs in the inlet and outlet regions than in the fully-developed MHD region for the reason mentioned in Chap. 1. On the other hand, a smaller Lorentz force may act in the flow direction and thus a small pressure recovery may occur in the first section of the inlet region and in the last section of the outlet region also for the reason mentioned in Chap. 1. The pressure drop behavior is not completely symmetric, since the fully- developed non-MHD flow enters the calculation domain in the inlet-region while the fully-developed MHD flow enters the domain in the outlet-region.

Figure 8 presents pressures along z-axis for the magnetic-field inlet-region, calculated by the authors and presnted in a previous paper (Kumamaru et al, 2007). The calculation parameters for Fig. 8 are the same as for Fig. 2, except for the Hartmann number change along z-axis. The Hartmann number (relating to the applied magnetic field) is 0 from z=0 to $z1$, increases linearly from z=$z1$ to $z2$, and is 100 from z=$z2$ to $z0$. The pressure change for the case of $z1/z2$=10/12, i.e. a standard case, in the inlet region, indicated by a dotted line, is also compared with the corresponding case in the outlet region in Fig. 3.

The pressure decreases slowly following the drop in a non-MHD laminar flow from z=0 to $z \approx z1$. The pressure recovery appears clearly in the region near $z \approx z1$. The pressure decreases more rapidly in the region from $z \approx z1$ to $z \approx z2$ than in the fully-developed MHD region of z>$z2$. The pressure decreases rapidly following the drop of a fully-developed MHD flow in the region of z>$z2$.

Figure 9 illustrates induced electric current distribution in the x-z plane at y=0 for the case of $z1/z2$=10/12, i.e. the standard case, in the magnetic-field inlet-region. The distribution in the

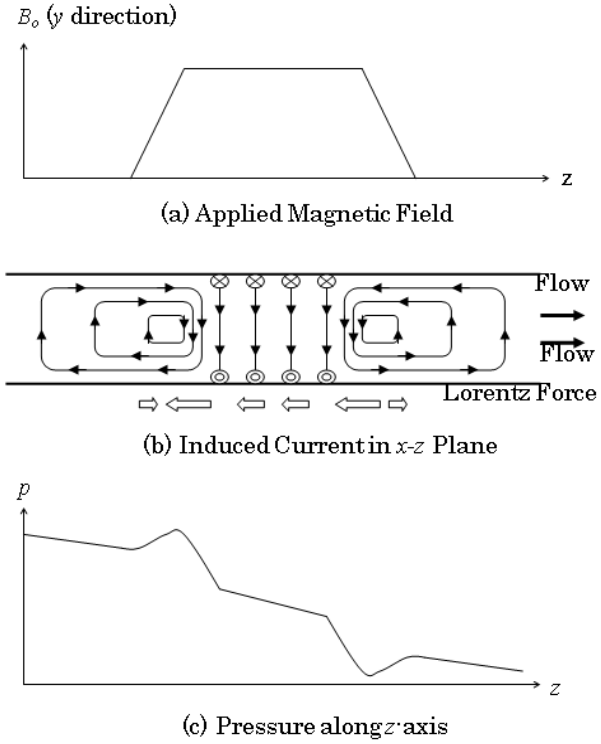

Fig. 7. Inlet and outlet regions of magnetic field.

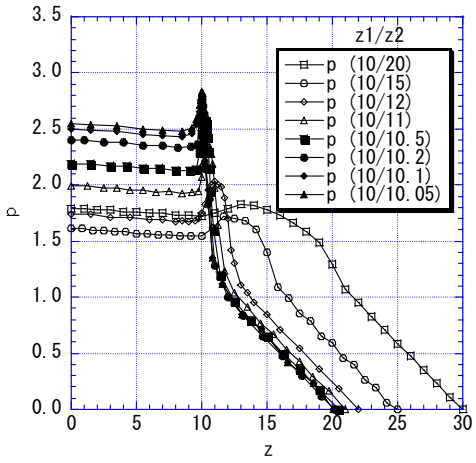

Fig. 8. Pressures along z-axis for magnetic-field inlet-region.

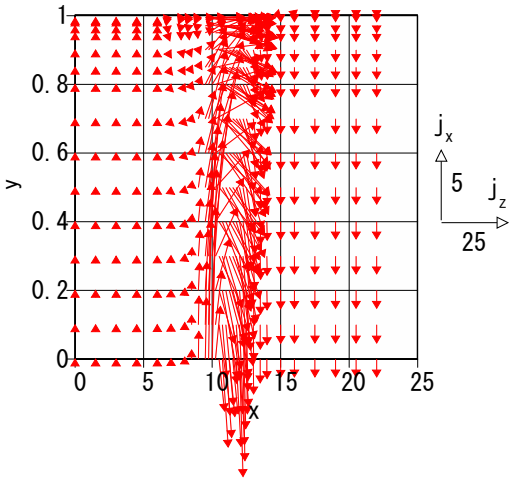

Fig. 9. Induced currents for magnetic-field inlet-region.

inlet region, Fig. 9, and that in the outlet region, Fig. 4, are nearly symmetric. For this reason, the sharp pressure drop in the inlet region from $z \approx 11$ to $z \approx 13$, i.e. $-\Delta p \approx 0.9$, agrees nearly with that in the outlet region from $z \approx 9$ to $z \approx 11.5$, i.e. $-\Delta p \approx 0.9$. However, the pressure recovery in the inlet region from $z \approx 9.5$ to $z \approx 11$, i.e. $-\Delta p \approx 0.4$ is larger than that in the outlet region from $z \approx 11.5$ to $z \approx 12$, i.e. $-\Delta p \approx 0.2$. The reason is examined later.

Figures 10(a), (b) and (c) show calculated velocity v_z distributions at z=10, 11 and 12, respectively, for the case of $z1/z2$=10/12, i.e. the standard case, in the magnetic-field inlet-region. The velocity profile at z=10, shown in Fig. 10(a), still keeps nearly a distribution typical to a non-MHD fully-developed laminar flow with a peak value of ~2. Hereafter, the velocity distribution becoms flatter along the channel axis, i.e. the z-axis, as shown in Figs. 10(b) (at z=11) and 10(c) (at z=12). However, the M-shape profile with extreme flow suppression in the fluid bulk region observed in the outlet region, as shown in Figs. 6(c) and (d), is not seen in the inlet region, as shown in Figs. 10(b) and (c). The reason may be that the non-MHD fully-develloped flow with the parabolic plofile enters the inlet region though the MHD fully-developed flow with the flat profile comes into the outlet region.

It is considered that, in addition to the pressure recovery due to the induced current in the positive x-direction, the velocity decrease in the fluid central region results in the pressure increase of $\Delta p \approx 0.4$ in $9.5<z<11$ of the magnetic-field inlet-region. On the other hand, it can be considered that after the pressure recovery of $\Delta p \approx 0.4$ due to the induced current in the positive x-direction, the pressure decreases by $-\Delta p \approx 0.3$ due to the velocity increase in $11.5<z<12$ of the magnetic-field outlet-region. From these differences, the pressure drop through the inlet region may become smaller than that through the outlet region.

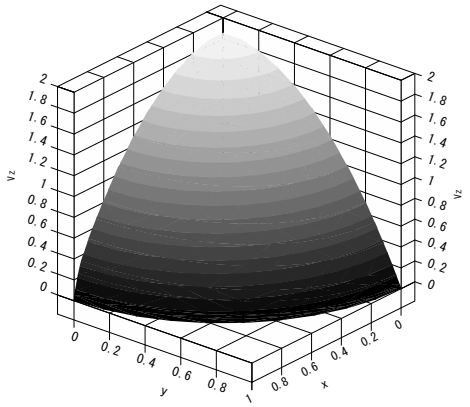

(a) At z=10

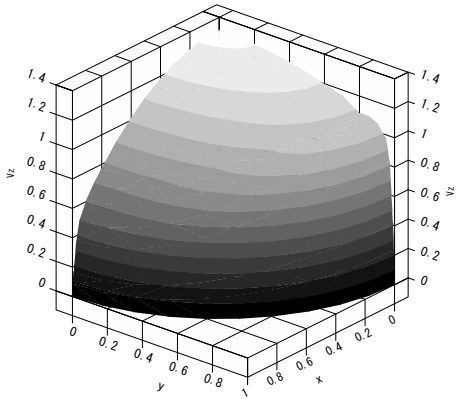

(b) At z=11

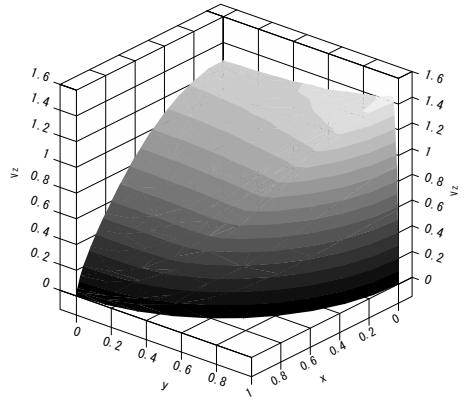

(c) At z=12

Fig. 10. Velocity distribution for magnetic-field inlet-region.

4. Conclusion

Three-dimensional numerical analyses have been performed on liquid-metal magnetohydrodynamic (MHD) flow through a circular pipe in the outlet region of magnetic field. The following conclusions have been obtained from the calculation results.

a. Along the flow axis, i.e. the circular pipe axis, the pressure decreases steeply as a fully-developed MHD flow, drops more sharply in the magnetic-field outlet-region, and finally decreases slowly as a normal fully-developed non-MHD flow.
b. If examined in detail, in the magnetic-field outlet-region, after the pressure drops most sharply, it recovers once and thereafter it drops sharply again outside the magnetic-field region.
c. The first sharp pressure drop and temporary pressure recovery are due to the formation of induced current loop which circulates in passing in the region downstream the magnetic-field region. The second sharp pressure drop is attributable to the change in velosity distribution outside the magnetic-field region.
d. The distribution of velocity in main flow direction changes from a flat profile of a fully-developed MHD flow, to an M-shaped profile and finally to a parabolic profile of a fully-developed non-MHD flow.
e. The total pressure drop through the magnetic-field outlet-region becomes larger than the corresponding drop through the magnetic-field inlet-region. The main reason may be that the difference in velocity profile change between the outlet region and the inlet region.

5. References

Aitov, T.N., Kalyutik, A.I. & Tananaev, A.V. (1983). Numerical Analysis of Three-Dimensional MHD-Flow in Channels with Abrupt Change of Cross Section, *Magnetohydrodynamics*, Vol. 19, pp. 223-229, ISSN 0024-998x

Asada, C. et al. Ed. (2007). *Handbook of Nuclear Engineering*, Ohmsha, Ltd., ISBN 978-4-274-20443-2, Tokyo, Japan [In Japanese]

Kalis, K.E. & Tsinober, A.B. (1973). Numerical Analysis of Three Dimensional MHD Flow Problems, *Magnetohydrodynamics*, Vol. 2, pp. 175-179, ISSN 0024-998x

Khan, S. and Davidson, J. N. (1979). Magneto-hydrodynamic Coolant Flows in Fusion Reactor Blankets, *Annals of Nuclear Energy*, Vol. 6, pp. 499-509, ISSN 0306-4549

Kumamaru, H. & Fujiwara, Y. (1999). Pressure Drops of Magnetohydrodynamic Flows in Rectangular Channel with Small Aspect Ratio and Circular Pipe for Very-Large Hartmann Numbers, *Proceedings of JSME/ ASME/SFEN 7th International Conference on Nuclear Engineering (ICONE-7)*, Tokyo, Japan, April 1999

Kumamaru, H., Shimoda, K. & Itoh, K. (2007). Three-Dimensional Numerical Calculations on Liquid-Metal Magnetohydrodynamic Flow through Circular Pipe in Magnetic-Field Inlet-Region, *J. of Nuclear Science and Technology*, Vol. 44, No. 5, pp. 714-722, ISSN 0022-3131 & 1881-1248

Leboucher, L. (1999). Monotone Scheme and Boundary Conditions for Finite Volume Simulation of Magnetohydrodynamic Internal Flows at High Hartmann Number, *J. of Computational Physics*, Vol. 150, pp. 181-198, ISSN 0021-9991

Lielausis, O. (1975). Liquid-Metal Magnetohydrodynamics, *Atomic Energy Review*, Vol. 13, pp. 527-581, ISSN 0004-7112

Moreau, R. (1990). *Magnetohydrodynamics*, Kluwer Academic Publishers, ISBN 978-90-481-4077-0, Dordrecht-Boston-London, Netherlands-USA-England

Schercliff, J.A. (1956). The Flow of Conducting Fluids in Circular Pipes under Transverse Magnetic Fields, *J. of Fluid Mechanics*, Vol. 1, pp. 644-666, ISSN 0022-1120

Sterl, A. (1990). Numerical Simulation of Liquid-Metal MHD Flows in Rectangular Ducts, *J. of Fluid Mechanics*, Vol. 216, pp. 161-191., ISSN 0022-1120

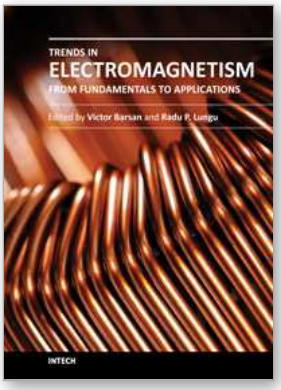

Trends in Electromagnetism - From Fundamentals to Applications
Edited by Dr. Victor Barsan

ISBN 978-953-51-0267-0
Hard cover, 290 pages
Publisher InTech
Published online 23, March, 2012
Published in print edition March, 2012

Among the branches of classical physics, electromagnetism is the domain which experiences the most spectacular development, both in its fundamental and practical aspects. The quantum corrections which generate non-linear terms of the standard Maxwell equations, their specific form in curved spaces, whose predictions can be confronted with the cosmic polarization rotation, or the topological model of electromagnetism, constructed with electromagnetic knots, are significant examples of recent theoretical developments. The similarities of the Sturm-Liouville problems in electromagnetism and quantum mechanics make possible deep analogies between the wave propagation in waveguides, ballistic electron movement in mesoscopic conductors and light propagation on optical fibers, facilitating a better understanding of these topics and fostering the transfer of techniques and results from one domain to another. Industrial applications, like magnetic refrigeration at room temperature or use of metamaterials for antenna couplers and covers, are of utmost practical interest. So, this book offers an interesting and useful reading for a broad category of specialists.

How to reference
In order to correctly reference this scholarly work, feel free to copy and paste the following:

Hiroshige Kumamaru, Kazuhiro Itoh and Yuji Shimogonya (2012). Three-Dimensional Numerical Analyses on Liquid-Metal Magnetohydrodynamic Flow Through Circular Pipe in Magnetic-Field Outlet-Region, Trends in Electromagnetism - From Fundamentals to Applications, Dr. Victor Barsan (Ed.), ISBN: 978-953-51-0267-0, InTech, Available from: http://www.intechopen.com/books/trends-in-electromagnetism-from-fundamentals-to-applications/three-dimensional-numerical-analyses-on-liquid-metal-magnetohydrodynamic-flow-through-circular-pipe-

INTECH
open science | open minds

InTech Europe
University Campus STeP Ri
Slavka Krautzeka 83/A
51000 Rijeka, Croatia
Phone: +385 (51) 770 447
Fax: +385 (51) 686 166
www.intechopen.com

InTech China
Unit 405, Office Block, Hotel Equatorial Shanghai
No.65, Yan An Road (West), Shanghai, 200040, China
中国上海市延安西路65号上海国际贵都大饭店办公楼405单元
Phone: +86-21-62489820
Fax: +86-21-62489821